UCRL-TR-216081

LAWRENCE
LIVERMORE
NATIONAL
LABORATORY

The Vetter-Sturtevant Shock Tube Problem in KULL

M. S. Ulitsky

October 11, 2005

This work was performed under the auspices of the U.S. Department of Energy by University of California, Lawrence Livermore National Laboratory under Contract W-7405-Eng-48.

The Vetter-Sturtevant Shock Tube Problem in KULL

Mark Ulitsky AX-Division   L-023

The goal of the EZturb mix model in KULL is to predict the turbulent mixing process as it evolves from Rayleigh-Taylor, Richtmyer-Meshkov, or Kelvin-Helmholtz instabilities. In this report we focus on an example of the Richtmyer-Meshkov instability (which occurs when a shock hits an interface between fluids of different densities) with the additional complication of reshock. The experiment by Vetter & Sturtevant (VS) [1], involving a Mach 1.50 incident shock striking an air / SF_6 interface, is a good one to model, now that we understand how the model performs for the Benjamin shock tube [2] and a prototypical incompressible Rayleigh-Taylor problem [3]. The x-t diagram for the VS shock tube is quite complicated, since the transmitted shock hits the far wall at ~ 2 millisec, reshocks the mixing zone slightly after 3 millisec (which sets up a release wave that hits the wall at ~ 4 millisec), and then the interface is hit with this expansion wave around 5 millisec. Needless to say, this problem is much more difficult to model than the Bejamin shock tube.

In Kull, the EZturb k- ε model [2-4] is tightly coupled to the Lagrange hydro, and so the actual mix model equations we solve when the model is active are:

$$\frac{d\alpha_r}{dt} = \frac{\partial}{\partial x_j}\left(\frac{\mu_t}{\sigma_M}\frac{\partial}{\partial x_j}\left(\frac{\alpha_r}{\rho}\right)\right)$$

$$\frac{d\alpha_r\rho_r}{dt} = \frac{\partial}{\partial x_j}\left(\frac{\mu_t}{\sigma_M}\frac{\partial}{\partial x_j}\left(\frac{\alpha_r\rho_r}{\rho}\right)\right)$$

$$\frac{d\rho u_i}{dt} = -\frac{\partial \tau_{ij}}{\partial x_j}$$

$$\frac{d\alpha_r\rho_r I_r}{dt} = \frac{\partial}{\partial x_j}\left(\frac{\mu_t}{\sigma_U}\frac{\partial}{\partial x_j}\left(\frac{\alpha_r\rho_r I_r}{\rho}\right)\right) + P_r^I + \delta_{I,Diss}\alpha_r\rho_r\varepsilon$$

$$\frac{d\rho k}{dt} = \frac{\partial}{\partial x_j}\left(\frac{\mu_t}{\sigma_K}\frac{\partial k}{\partial x_j}\right) - \tau_{ij}S_{ij} - \rho\varepsilon + P$$

$$\frac{d\rho\varepsilon}{dt} = \frac{\partial}{\partial x_j}\left(\frac{\mu_t}{\sigma_Z}\frac{\partial \varepsilon}{\partial x_j}\right) - C_{1\varepsilon}\tau_{ij}S_{ij}\frac{\varepsilon}{k} - C_{2\varepsilon}\rho\frac{\varepsilon^2}{k} + C_{3\varepsilon}P\frac{\varepsilon}{k} \quad .$$

Here, α_r, ρ_r, and I_r are the volume fraction, thermodynamic density, and specific internal energy (by mass) for material r. S_{ij} is the strain rate tensor, and τ_{ij} is the turbulent shear stress tensor, for which we use the following Boussinesq approximation:

$$\tau_{ij} = \delta_{Iso} \frac{2}{3} \rho k \delta_{ij} - \delta_{Anso} 2\mu_t \left(S_{ij} - \frac{\delta_{ij}}{3} \frac{\partial u_k}{\partial x_k} \right) \quad .$$

The turbulent viscosity includes the effects of both shear and buoyancy and takes the form:

$$\mu_t = C_\mu \rho \frac{k^2}{\varepsilon} + C_\omega \rho \frac{k^3}{\varepsilon^2} \sqrt{\omega^2 + \frac{\nabla p \cdot \nabla p}{p\rho} - \frac{\nabla p \cdot \nabla \rho}{\rho^2} \left[1 - \Theta(\nabla p \cdot \nabla \rho) \right]} \quad .$$

The unlimited form of the buoyant production term is given by:

$$P = -\frac{\mu_t}{\sigma_\rho \rho^2} \nabla p \cdot \nabla \rho$$

and the way this term manifests itself in the internal energy equation is:

$$P_r^I = -h_r p_r \nabla \cdot \left(\frac{\mu_t}{\sigma_\rho \rho^2} \nabla \rho \right) \quad .$$

The model constants are $C_{1\varepsilon}$, $C_{2\varepsilon}$, $C_{3\varepsilon}$, σ_M, σ_U, σ_K, σ_Z, σ_ρ, C_μ, and C_ω. Also, δ_{Iso}, δ_{Aniso}, and $\delta_{I,diss}$ are on/off switches that can be set to 1 or 0. To simplify the form of the turbulent viscosity and the Reynolds stress, we will set $C_\omega = 0$ and $\delta_{Aniso} = 0$ for this problem.

In previous reports [2-4], we have not focused too much on the form of the buoyant production term or pointed out when it is active/inactive. For this problem however, we need to consider the production term in more detail. First, let's start by considering the sign of the production term (denoted by *P* in the k and ε transport equations above) under the influence of RT and RM. When an interface is RT unstable, the pressure and density gradients will be in different directions, and *P* will therefore be positive (note the negative sign in front of the density and pressure gradients). A positive value for *P* will increase k and ε, □□□□□□□□□□□□□, □□□□□□□□□□□□□□□□□□□□□□□□□□□□□□. For the RT stable case, we don't want to promote interfacial growth unless a shock is present. Therefore, we must be able to detect when a shock is present in a zone, and also make sure that the production term has the correct sign for the RT stable case (note that a naïve treatment would have k and e decreasing for this case, as the production term would be negative). To simplify this process and also to make sure that we treat the PdV work term in the internal energy equations correctly, it will be useful to consider a velocity **a**, which is defined as:

$$\mathbf{a} = -\frac{\mu_T \nabla \rho}{o_\rho \rho^2} \quad .$$

Thus, for RT unstable interfaces, we do nothing to **a** (whether or not a shock is present). For RT stable interfaces with a shock, we flip the sign of **a**, and for RT stable interfaces without a shock, we set **a** = 0. To determine if a shock is present in a zone, we compute a simple ratio of an artificial pressure to the zone pressure. If this value is above a user-defined threshold, then the Boolean shock detection flag switches from false to true.

We are given that the incident Mach number is 1.50 and that the ambient pressure is 23 kPa. If we assume an ambient temperature of 70 degrees F and molecular weights for air and SF_6 of 28.94 g/mol and 146.05 g/mol respectively, then we can use the ideal gas law to calculate the ambient air and SF_6 densities to be 2.7207e-4 g/cm^3 and 1.37305e-3 g/cm^3 . With these values and the standard 1D shock relations [5-6], we can compute shocked values for the air (we assume γ_{air} = 1.4). Thus the shocked air density, pressure, and velocity are found to be 5.0662e-4 g/cm^3, 5.65416e6 dynes/cm^2, and 2.3890e4 cm/sec. A spatial domain of 218 cm was selected, since this length ensures that the initial rarefaction transmitted into the air (which reflects off the left moving Lagrangian boundary), never gets too close to the mixing zone. To run the problem further in time than ~5.3 millisec would require lengthening the shock tube. It was decided that for initial testing with this problem, that 800 zones would be sufficient to cover the 218 cm. This results in 224 zones being used to cover the experimental test section of 61 cm, with the remaining zones being used to obtain the correct boundary behavior and also ensure that no shocks or rarefactions strike the mixing zone from the left hand side.

For the Benjamin problem [2], it was seen that the choice of artificial viscosity had virtually no effect on the growth of the mixing zone. This is not the case for the VS problem, however, due to the much more complicated shock dynamics and interactions with the mixing zone. Figure 1 shows density profiles at t = 1 millisec (before the shock has hit the far wall) obtained using different Q's. Clearly, the ScalarQ (a standard VonNeumann-Richtmyer Q with linear and quadratic parts) with linear and quadratic coefficients set to 2 and 8/3 has some problems. Basically, with these coefficients, there is a considerable amount of shock heating which causes the density to drop and the shock speed to increase. Here the mixing zone is located at x = ~170 cm, while the shock front is somewhere between 180 –185 cm. The figure also shows a problem with the rarefaction that is heading towards the Lagrangian boundary. Interestingly enough, these problems go away when the zoning is doubled. The hyperviscosity Q [7] does a great job at 800 zones. This is the first time that this Q has been run on a multi-material problem, and as Figure 2 demonstrates, the results are nearly identical to the default Q in KULL, namely the CSWEdgeQ [8] with advection limiter.

Figure 3 shows the effect of changing the linear and quadratic coefficients for the ScalarQ. While reducing the coefficients certainly improves the shock timings, it is not clear whether there is a choice for the coefficients at 800 zones that will capture the shock and rarefaction satisfactorily. Therefore, we have decided to use the hyperQ for running this problem. Figure 4 shows the SF_6 volume fraction profiles with 2 and 8/3 for the coefficients. Clearly, if we want to run with only 800 zones, the hyperQ does a much better job of resolving the mixing zone. Since the mixing zone widths are being computed in the code by interpolating the volume fractions, we would prefer a method that really resolves the mixing.

Figure 5 shows a comparison of the mixing zone widths between the code and the experimental data. The value of the model coefficients used to match the data in this figure are given by :

$\sigma_M = \sigma_\rho = \sigma_U = \sigma_K = .7$, $\sigma_e = 1.3$, $c_\mu = .09$, $c_{\varepsilon 1} = 1.44$, $c_{\varepsilon 2} = 1.92$, $c_{\varepsilon 3} = 1.1$, $\delta_{iso} = 1$, $\delta_{aniso} = 0$, $\delta_{I,diss} = 1$.

The initial values for k and L (from which we infer ε) are .01 v^2, where v is the speed of the shocked air given earlier and .083 cm. Several points are worth noting in this figure. First, the initial values for k and L were chosen to match the pre-reshock data, and whether shock detection is on or off has no effect on these values. Second, having shock detection turned on is crucial to capturing the correct post –reshock physics. That is, if shock detection is off, then no kinetic energy or dissipation will be produced by the buoyant production term and at reshock, the kinetic energy in the mixing zone will be substantially less than if shock detection is active. Also, the threshold for shock detection (the ratio of the artificial to the zone pressure) was set to .005, and this value was arrived at by plotting this dimensionless ratio as a function of position at several times before the shock reached the far wall. Note that in computing the artificial pressure, we used a conservative estimate of the zone size which gives a value of ~ $\Delta x/2$ for 1D problems, where Δx is the width of the zone (distance between the nodes in the x-direction). Therefore, if we used the actual zone size, the threshold value would be closer to .02. What the figure suggests is that when we are accounting for the buoyant production term, we are producing too much kinetic energy, and thus, too much mixing.

Figure 6 shows the effect of increasing σ_ρ from .7 to 1.4. Since σ_ρ is in the denominator of the production term, this will decrease the amount of mixing. Much better agreement for the post-reshock data is obtained without sacrificing any of the agreement at earlier times. Clearly, a larger choice for this constant will match the data even better. We need to be careful however, as a convergence study has not been performed, and so we do not know how much smaller the computed widths will become. Figure 7 addresses this question by looking at results with 400, 800, and 1600 zones. The numbers in parentheses are the number of zones that are in the 61 cm test section. Thus, it appears we still have a ways to go before we reach true convergence. This means that a value of σ_ρ around 1.0 will probably best match the data. It should also be mentioned that there is an unknown distance between the test section and the membrane initially separating the two gases. This distance has been estimated to be ~ 1cm, and therefore it is possible that using 62 cm for the test section would give better results.

References:

[1] M. Vetter & B. Sturtevant, *Experiments on the Richtmyer-Meshkov instability of an air/SF6 interface*, Shock Waves, **4**, pp. 247-252, 1995.

[2] M. Ulitsky, *The Benjamin Shock Tube Problem in KULL*, UCRL-TR-214888.

[3] M. Ulitsky, *An Incompressible Rayleigh-Taylor Problem in KULL*, UCRL-TR-215627.

[4] M. Ulitsky, *The Barenblatt Turbulent Burst Problem in KULL*, UCRL-TR-212637.

[5] F. Harlow and A. Amsden, Fluid Dynamics – A LASL Monograph, LA-4700, 1971.

[6] J. Anderson, *Modern Compressible Flow*, McGraw-Hill, 1990.

[7] M. Ulitsky, *A Tensor Hyperviscosity Model in KULL*, UCRL-TR-213310.

[8] E.J. Caramana, M.J. Shashkov, and P.P. Whalen, *Formulations of Artificial Viscosity for Multi-dimensional Shock Wave Computations*, JCP, **144**, p. 70-97, 1998.

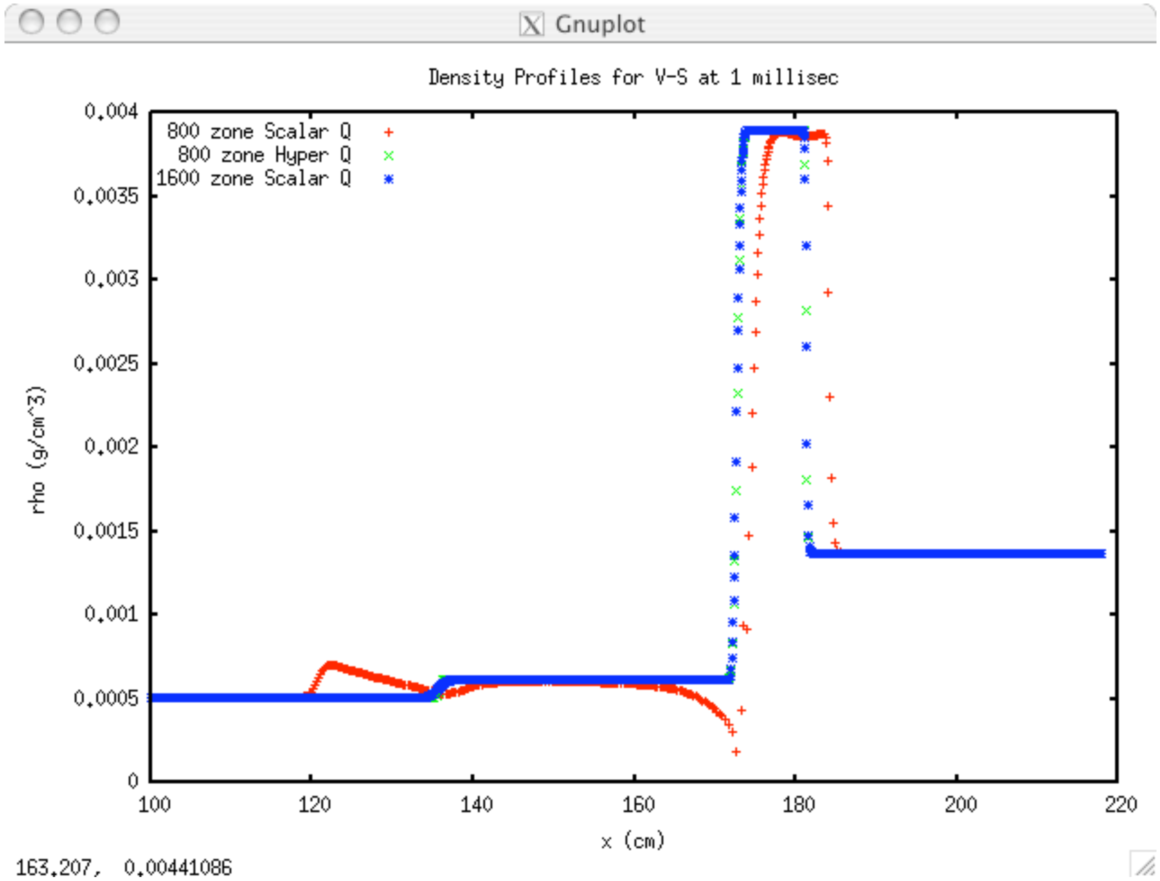
Gnuplot
Density Profiles for V-S at 1 millisec
800 zone Scalar Q
800 zone Hyper Q
1600 zone Scalar Q
rho (g/cm^3)
x (cm)
0.004
0.0035
0.003
0.0025
0.002
0.0015
0.001
0.0005
0
100
120
140
160
180
200
220
163.207, 0.00441086

Figure 1

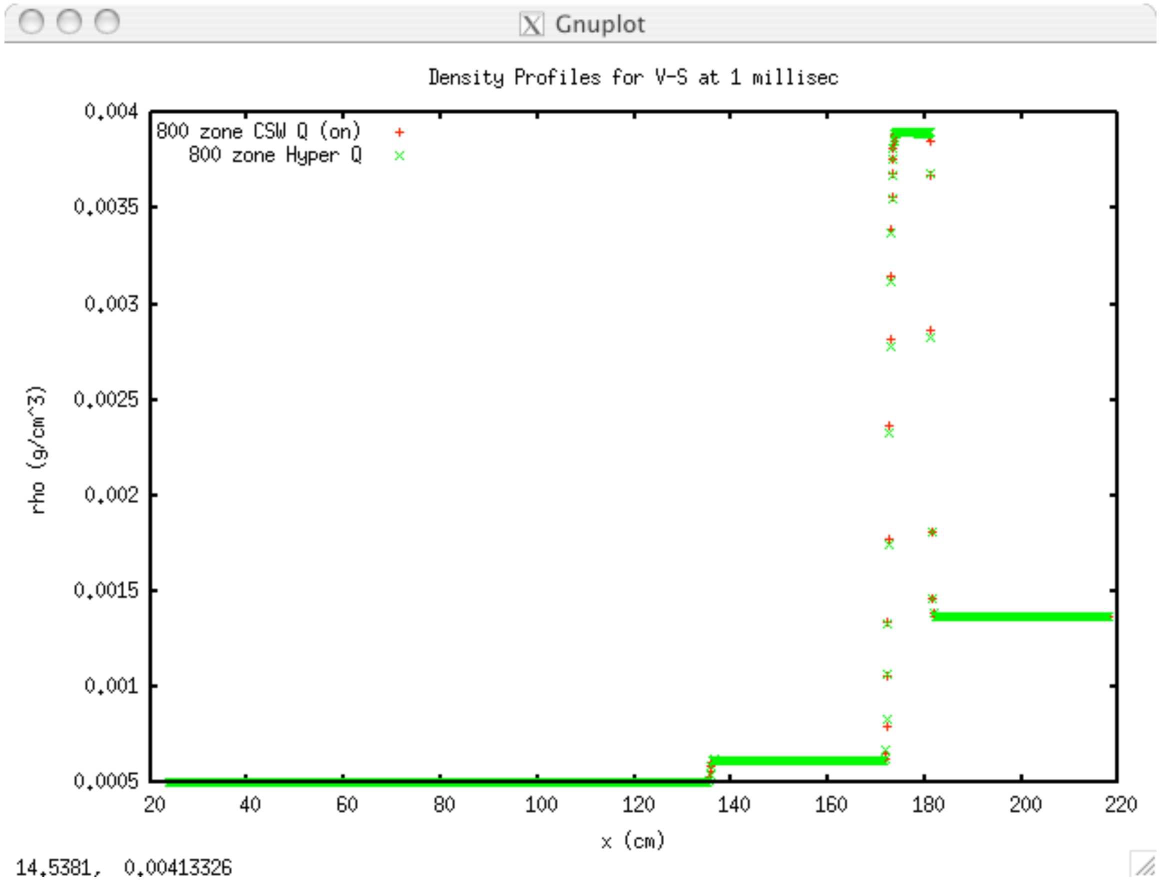

Gnuplot
Density Profiles for V-S at 1 millisec
800 zone CSW Q (on)
800 zone Hyper Q
0.004
0.0035
0.003
0.0025
0.002
0.0015
0.001
0.0005
rho (g/cm^3)
20
40
60
80
100
120
140
160
180
200
220
x (cm)
14.5381, 0.00413326

Figure 2

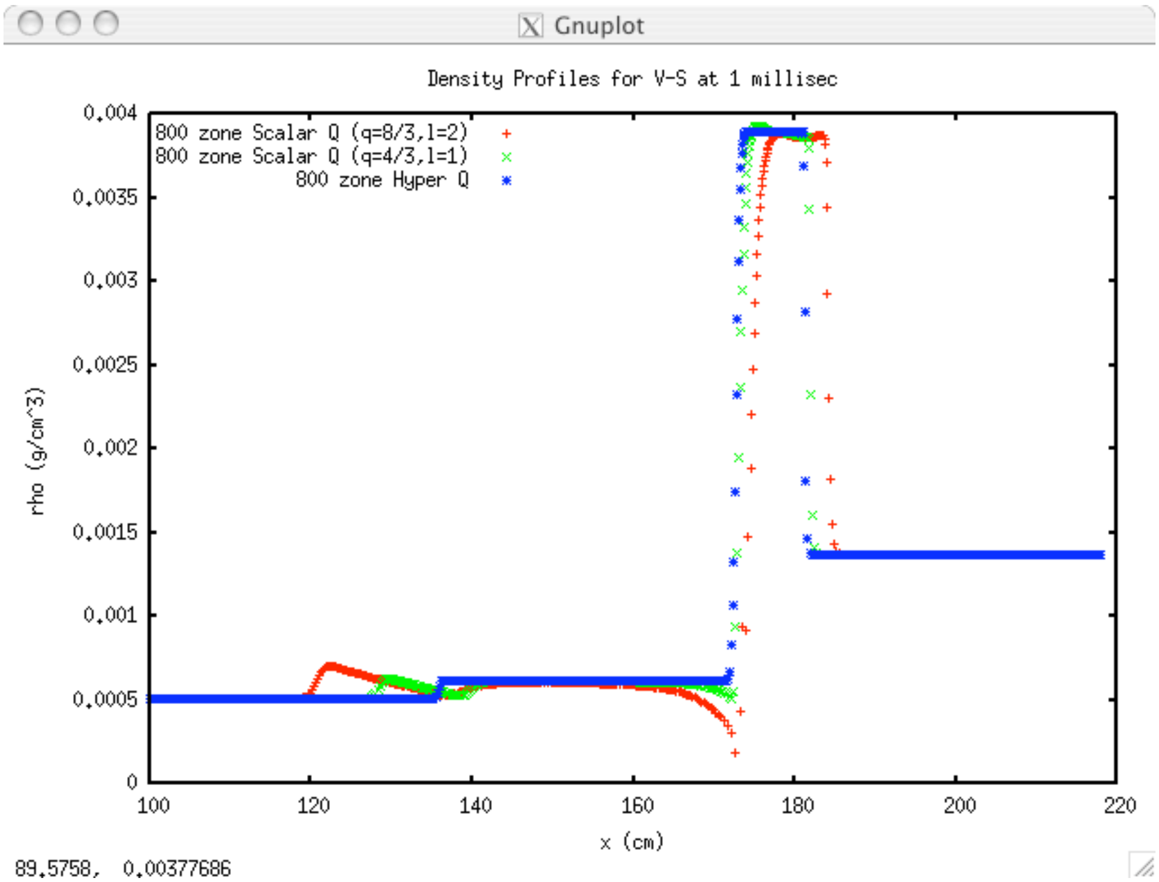
Gnuplot
Density Profiles for V-S at 1 millisec
800 zone Scalar Q (q=8/3,l=2)
800 zone Scalar Q (q=4/3,l=1)
800 zone Hyper Q
rho (g/cm^3)
x (cm)
0.004
0.0035
0.003
0.0025
0.002
0.0015
0.001
0.0005
0
100
120
140
160
180
200
220
89.5758, 0.00377686

Figure 3

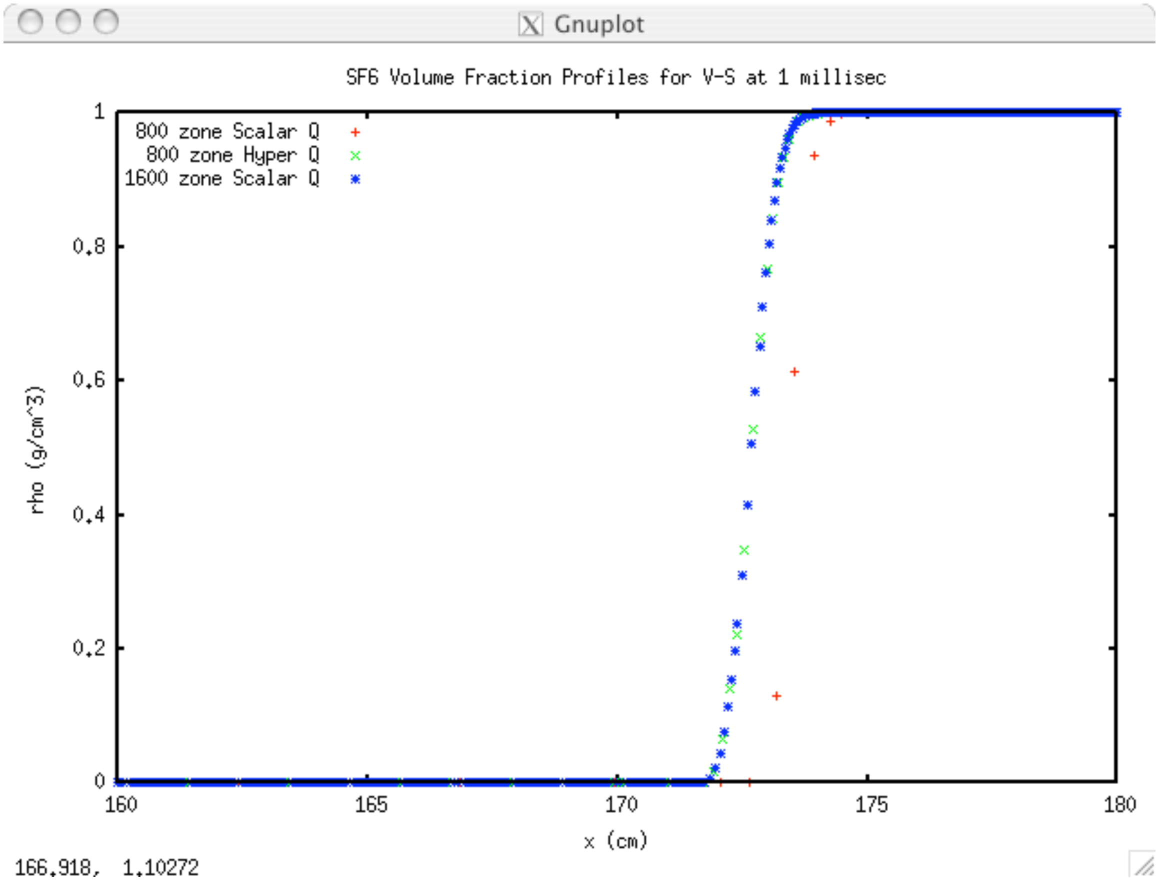
Gnuplot
SF6 Volume Fraction Profiles for V-S at 1 millisec
800 zone Scalar Q
800 zone Hyper Q
1600 zone Scalar Q
rho (g/cm^3)
x (cm)
0
0.2
0.4
0.6
0.8
1
160
165
170
175
180
166.918, 1.10272

Figure 4

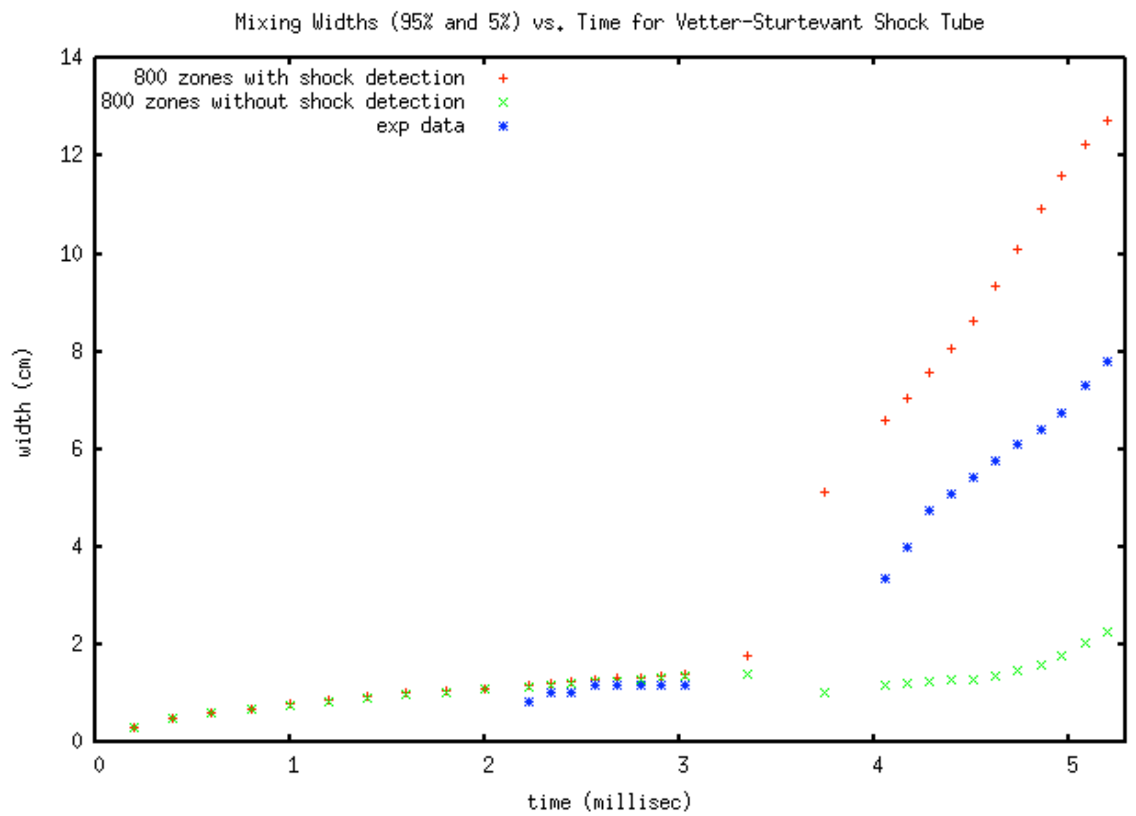
Mixing Widths (95% and 5%) vs. Time for Vetter-Sturtevant Shock Tube
800 zones with shock detection
800 zones without shock detection
exp data
width (cm)
time (millisec)
0
2
4
6
8
10
12
14
0
1
2
3
4
5

Figure 5

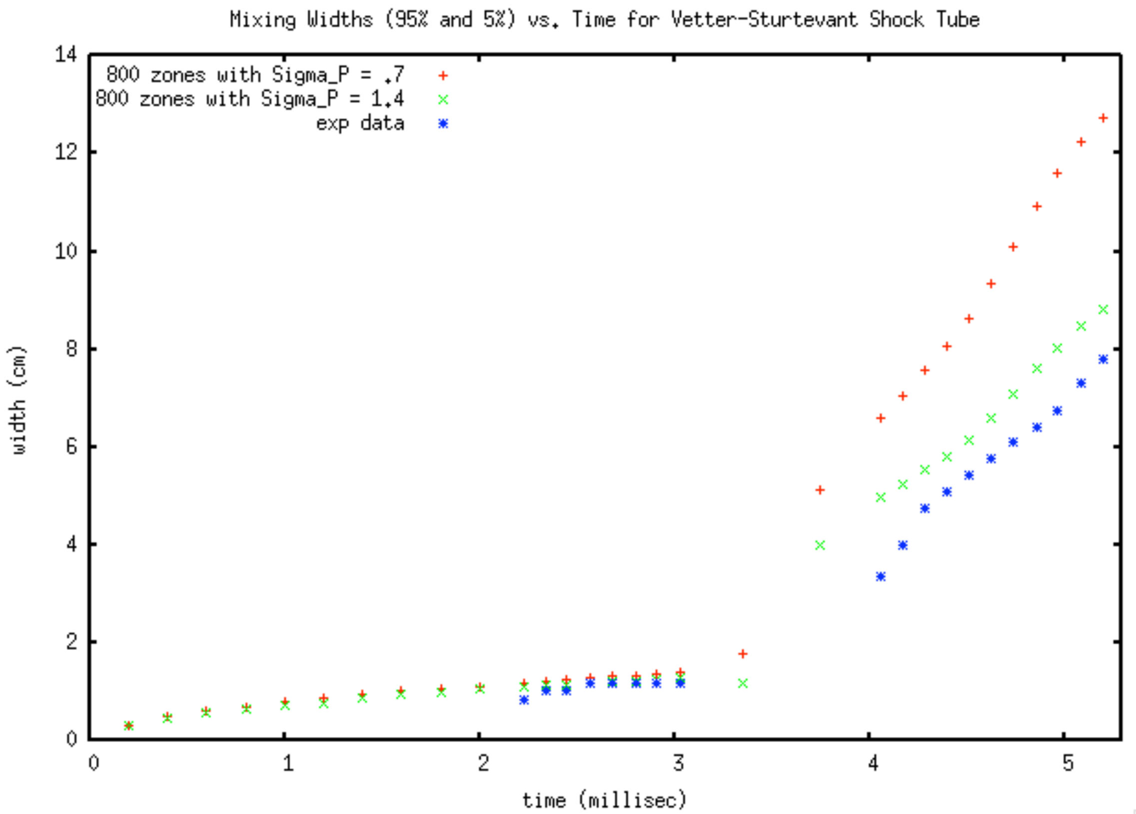
Mixing Widths (95% and 5%) vs. Time for Vetter-Sturtevant Shock Tube
800 zones with Sigma_P = .7
800 zones with Sigma_P = 1.4
exp data
width (cm)
time (millisec)
0
2
4
6
8
10
12
14
1
3
5

Figure 6

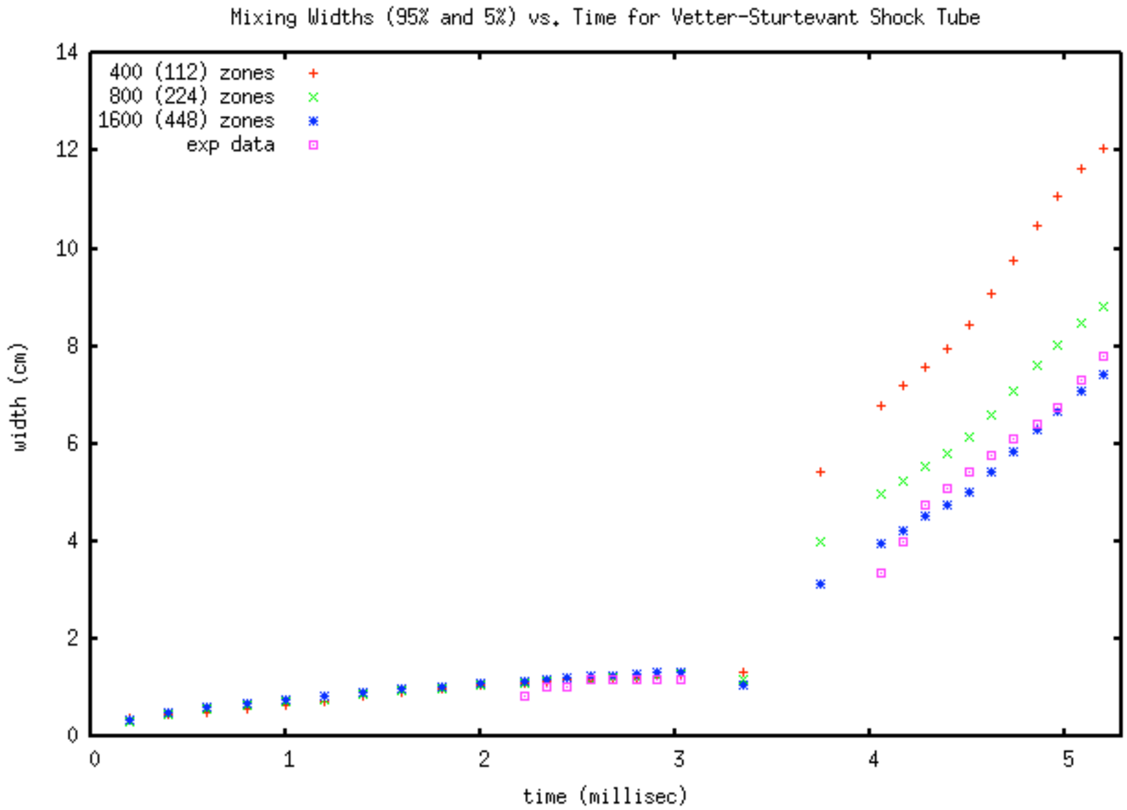
Mixing Widths (95% and 5%) vs. Time for Vetter-Sturtevant Shock Tube
400 (112) zones
800 (224) zones
1600 (448) zones
exp data
width (cm)
time (millisec)
0
2
4
6
8
10
12
14
0
1
2
3
4
5

Figure 7